Electronic Supplementary Material (ESI) for Chemical Communications
This journal is © The Royal Society of Chemistry 2013

Electronic Supplementary Information

Photocathodic behavior of ferroelectric $Pb(Zr,Ti)O_3$ films decorated with silver nanoparticles

Chunyan Wang, Dawei Cao, Fengang Zheng, Wen Dong, Liang Fang, and Mingrong Shen*

Department of Physics and Jiangsu Key Laboratory of Thin Films, Soochow University, Suzhou 215006, People's Republic of China. Email: mrshen@suda.edu.cn

S1 : Experimental Section

PZT film prepared by Sol-gel method: A solution containing Pb, Zr and Ti elements was firstly prepared. The concentration of the solution was 0.2mol/L. Titanium butoxide (2.7229g) and zirconium butoxide (0.9077g) were mixed with 2-methoxyethanol. Lead acetate (4.1726g) was dissolved into the heated acetic acid and further heated to 110 °C to remove the associated water. When the temperature of Pb solution was decreased to 90 °C, the Zr–Ti mixture solution was added to Pb solution while stirred continuously for approximately 1h. Then the clear yellowish solution was prepared. Secondly, spin-coating was employed to deposit the filtered solution at 1000 rpm for 5s, then 3000 rpm for 25s onto the ITO/quartz substrates. After each spin-coating, the film was fired on a furnace at 150 °C and then inserted into a preheated tube furnace at 400 °C for 10min in ambient air. These procedures were repeated several times. The films were crystallized in oxygen under 650 ^{o}C for two hours. The thicknesses of PZT films were controlled through the multiple spin-coatings.

Ag nanoparticles fabricated by interrupted pulsed-electrodeposition method: Ag nanoparticles were fabricated onto PZT surface in the dark from a solution of 0.05M $AgNO_3$ in deionized water. Pulsed potential profiles starting from a potential of 0.2 V (0.1s) to a reduction potential of -0.8 V (0.1s) and back to 0.2 V (0.1s) (vs SCE) were applied to the working electrode for Ag deposition using a specifically designed software module. One period of deposition consists of 50 pulses. After one period of

This journal is © The Royal Society of Chemistry 2013

electrodeposition, the growth of Ag was interrupted and the sample was thoroughly rinsed with deionized water and dried in a nitrogen stream. Then the photocurrent was measured using an electrochemical workstation (CHI660D) with a 100 mW/cm^2 Xe lamp and 0.1M Na_2SO_4 as electrolyte. During the measurement, the as-prepared sample served as the working electrode, a Pt wire as the counter electrode, and a SCE electrode as the reference electrode. After PEC measurements, the sample was again thoroughly rinsed with deionized water and dried in a nitrogen stream. Another period of Ag growth was performed repeatedly. Unless otherwise stated, the number of the interrupted electrodeposition of Ag on PZT surface is 6. One obvious advantage of this procedure is that we can know how many periods for the deposition of Ag particles on PZT is the best for the PEC performance of Ag/PZT heterostructure.

Sample characterizations: The photocurrent was measured using an electrochemical workstation (CHI660D) with a 100 mW/cm^2 Xe lamp illumination and 0.1M Na_2SO_4 as electrolyte. During the measurement, the as-prepared sample served as the working electrode, a Pt wire as the counter electrode, and a SCE electrode as the reference electrode. The crystal structures of the films were evaluated by measuring x-ray diffraction (XRD) spectra with Ni filtered CuK_α radiation. Scanning electron microscope (SEM) surface and cross-section images are checked by Hitachi S-4700. Monochromatic incident photon-to-electron conversion efficiency (IPCE) was measured by IPCE/QE 200 of Newport within the wavelength of 300-700 nm. UV-visible light transmission and absorption characteristic were measured by JASCO UV/VIS 550. Polarization-voltage (P-V) hysteresis loops were examined using a precision ferroelectric analyzer from Radiant Technology. Ultraviolet photoelectron spectroscopy (UPS) data were obtained on a modified Physical Electronics photoemission system (Kratos Axis Utra Dld) that has been incorporated into a custom-built ultrahigh vacuum (UHV) with a base pressure of 10^{-10} Torr. A SPECS UVS 10/35 He lamp at 21.21 eV was used as UPS source. To measure the hysteresis loop of the PZT film, about 40 nm thick Pt dots with diameters of 0.28 mm were sputtered onto the PZT film. Hysteresis loops were then examined using a radiant precision ferroelectric analyzer.

S2: UPS spectra and the energy diagram of the PZT film

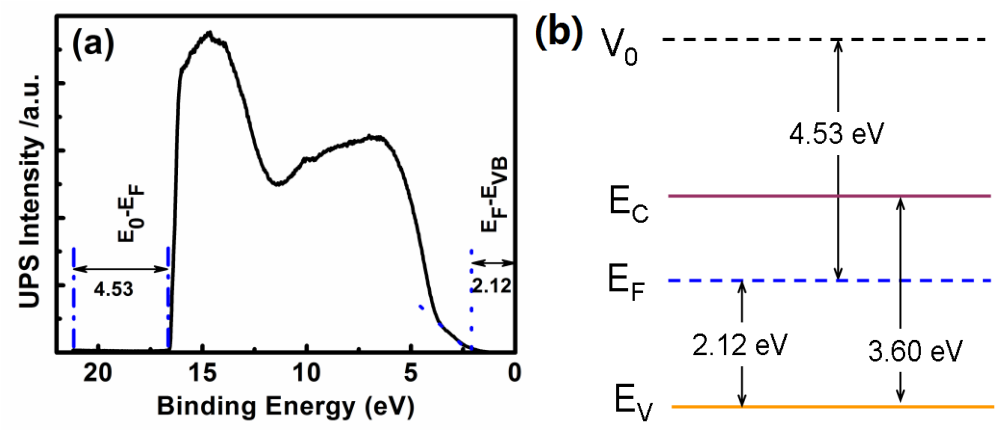

Fig. S1 (a) UPS spectra of the PZT film. The work functions (φ=V_O-E_F, V_O is the vacuum energy level, and E_F the Fermi level) can be derived from the low kinetic energy cut-offs in the secondary emission features, which is 21.21-16.78=4.53 eV. 21.21 eV is the photon energy of UV source (He I discharge). The valence band maximum energy E_V with respect to E_F is found extrapolated by the linear portion of the low binding energy side,[1] as indicated in the Figure. (b) Schematic energy diagram of the PZT film deduced by the UPS data. The band gap of PZT is measured to be about 3.60 eV by the UV-visible light transmission method. The surface of the PZT film is n-type with a relative low donor level, consistent with that reported.[2] Since the surface of the PZT films is n-type, the majority carriers, etc., electrons on the PZT surface will diffuse into the electrolyte when contacting PZT with the liquid. This leads to a depleted region and a barrier for electrons on the PZT surface with upward energy band. Because E_F is far away from the conduction band, the barrier is not so high and thus we call it a weak barrier.

S3: The advantage of the interrupted growth of Ag nanoparticles

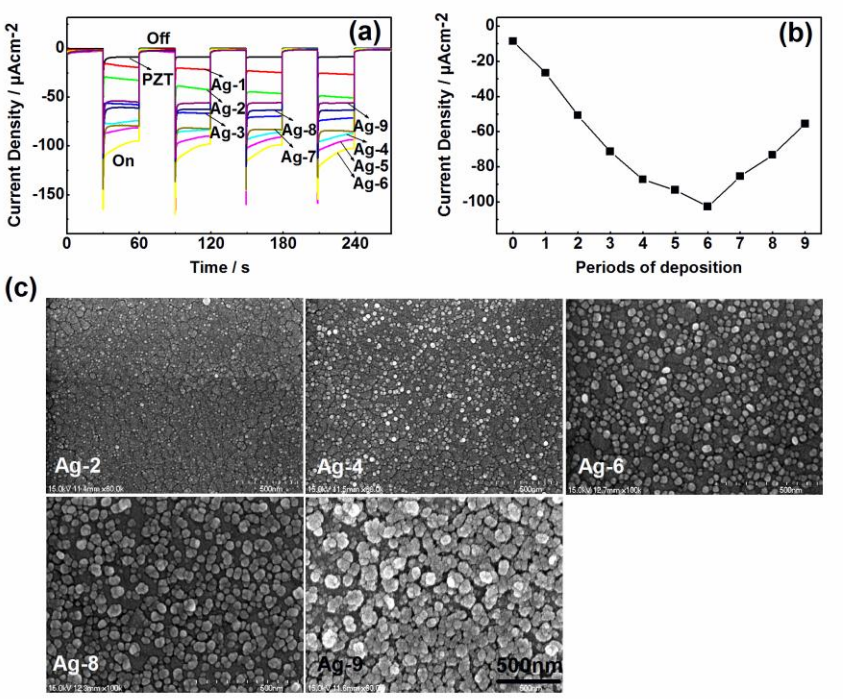

Fig. S2 (a) PEC response for the bare and Ag covered PZT samples under zero bias vs SCE under the irradiation of 100 mW/cm^2. Ag-n refers to the n periods interrupted deposition. (b) The steady-state photocurrent dependent of the deposition periods of Ag nanoparticles. The small difference within 3% on the photocurrent was found during the repeated experiments, however, the 6-period always results in the best PEC performance. Comparing with 6 cycles, 8 cycles only exhibits the increased particle size and density slightly on average. When the light comes from the quartz side, the ultraviolet light is absorbed by PZT film, and the left visible light will be scattering and/or trapping by the Ag nanoparticles. The scattered light will then acquire an angular spread in the dielectric that may come back to the Ag/PZT interface; and the trapping light produces a strong local field enhancement around the metal nanoparticles to increase absorption in a surrounding dielectric material. Both effects are dependent of the size and density of the metal nanoparticles [Nature Mater. 2010, 9, 205]. We propose that the six-period deposition results in the most suitable Ag particle size and density for the current study and therefore the best PEC performance for Ag-6/PZT sample. (c) The top view SEM images of the PZT film with the decoration of Ag nanoparticle fabricated under different interrupted periods.

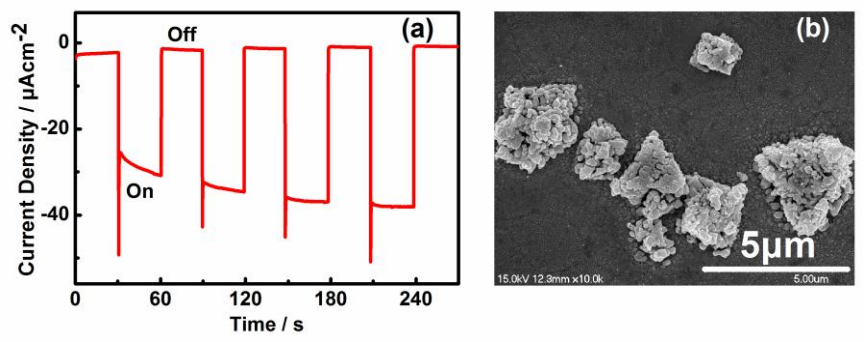

Fig. S3 (a) PEC response for the Ag/PZT sample where Ag is electrodeposited with 300 continuous pulses. (b) The corresponding SEM surface image. Large crystallites with size about 1 μm and stacked particle structure can be seen. In addition, the density of the crystallites is low, compared with the interrupted case where the same pulse numbers are used. The results manifest that in this case the Ag crystallites grow continuously or new particles nucleate on previously grown Ag particles. Less Ag nucleates on the fresh PZT surface in the continuous deposition mode.

In Figs. 2a, 2b and S3a, the photocurrent decays with time within a several seconds. Such transient photocurrent is ascribed to the surface recombination of the photogenerated electrons and holes [Chem. Commun. 2012, **48**, 2027]. The instantaneous current when the light is switching on is a measure of the flux of electrons in the surface. The subsequent decay towards the steady state current results from the capture of built-up electrons in surface states inducing a hole flux associated with recombination.

S4: The work function of the PZT/ITO mixture.

We obtained that the work function of PZT film is about 4.6 eV, as presented in Figure S1. The reported value of the vacuum work function of ITO thin films is about 4.5 eV.[3] However, different values ranging from 3.9 to 6.0 eV have been reported in the literature, and the work function of ITO is extremely sensitive to the state of a surface.[4-6] The enhancement of the work function of ITO can be fulfilled by adding a proper layer of dipoles just outside the ITO surface or mixing with $LaTiO_3$.[5,6] In this study, PZT film is crystallized on ITO electrode, and PZT/ITO contact experiences a

high temperature annealing process. Thus we assume that PZT and ITO are mixed on the interface, and a layer of dipoles may form just outside the ITO surface since PZT is highly polar. This may result in a larger work function of ITO than that of PZT. In order to check this point, we spin-coated a very thin PZT layer (about 10 nm) on ITO by controlling the mole ratio of PZT in 2-methoxyethanol [$CH_3OCH_2CH_2OH$] before coating. ITO/PZT is annealed under 650 ^{0}C in air in order to ensure their mixture. UPS measurement is then performed along with the pure ITO layer. The UPS results in Figure S4 illustrate that the work function of ITO/PZT is found to be about 0.4 eV larger than that of the pure ITO, confirming our above assumption that a barrier can be formed between PZT and ITO.

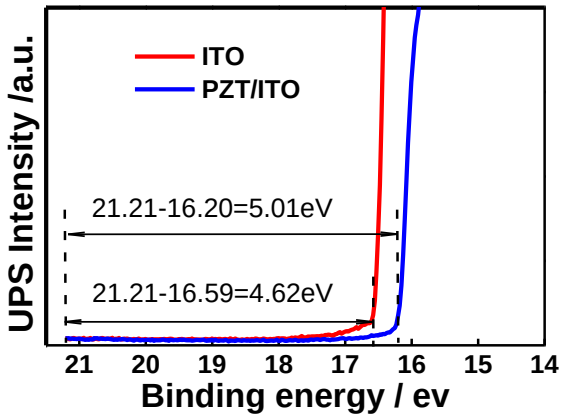

Fig. S4 UPS spectra of pure ITO and PZT/ITO surface. The low kinetic energy part is shown. The work functions can be derived from the low kinetic energy cut-offs in the secondary emission features, which is 4.62 eV for pure ITO, and 5.01 eV for PZT/ITO.

S5: Photocurrent vs. time under visible light.

From Fig. 2(c), we can see a broad peak between about 400 and 550 nm after the Ag nanoparticle decoration, indicating that a visible light photo-to-current conversion happens on the photocathode. In order to have a more clear demonstration that how many the photocurrent in Fig. 2(b) is originated from the visible light, we add two

filters during the measurements: one is JB400 and another is CB550 with absorption wavelength edges of 400 and 550 nm, respectively. The transmission spectra of these two filters are shown in the following as Fig S5(a).

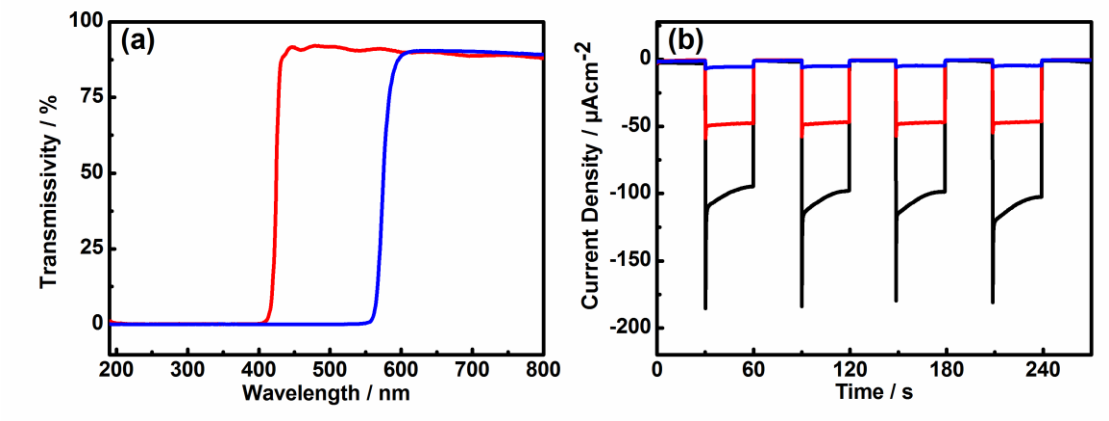

Fig. S5 (a) The transmission spectra of two filters: JB400 (red) and CB550 (blue). (b) The photocurrent of the Ag-6/PZT sample: without filter (black); with JB400 filter (red) and CB550 filter (blue), respectively.

In Fig S5(b), the black line is the photocurrent obtained without filter which has already shown in Fig. 2(b). The red line is the photocurrent after using the JB400 filter. About 50 $\mu A/cm^2$ is from the visible light. The photocurrent is close to zero after using the CB550 filter. Since the total stable photocurrent is about 100 $\mu A/cm^2$, the left part (100-50=50 $\mu A/cm^2$) can be originated from the light below 400 nm. Thus, we conclude that the huge enhancement of the PEC properties can not be ascribed to the broad IPCE peak at 452 nm solely. When the simulated sun light shines on the quart/ITO/PZT/Ag from the quartz side, ultraviolet light is directly absorbed in the PZT film, whereas poorly absorbed visible light is scattering and trapping by the Ag metal nanoparticles. Above results indicate that even the photocurrent originated from the light below 400 nm is significantly enhanced after Ag decoration (50 $\mu A/cm^2$ vs. 10 $\mu A/cm^2$). The light absorption below 400 nm is proposed to be nearly the same for the pure PZT and PZT/Ag samples because it is dominated by the PZT bandgap absorption, therefore the efficient separation of the photocarriers is expected in the PZT/Ag sample. We suggest that the improvement of energy level alignment for efficient electron-extraction is another main reason for the enhancement of the PEC

properties of the PZT/Ag sample, which is given as Fig. 3.

S6: The stability of the Ag/PZT photoelectrode after illumination.

For inorganic metal oxide, the materials with ABO_3 structure are usually stable since they are formed under relative high temperature generally above 600 ^{0}C. Fig. S6 shows the morphology (SEM) and constituent (XRD) of Ag-6/PZT surface after a long time (4 hours) continuous PEC measurement. Comparing with the original ones, we can see that both SEM and XRD patterns change little, indicating that the PZT and Ag are stable after illumination.

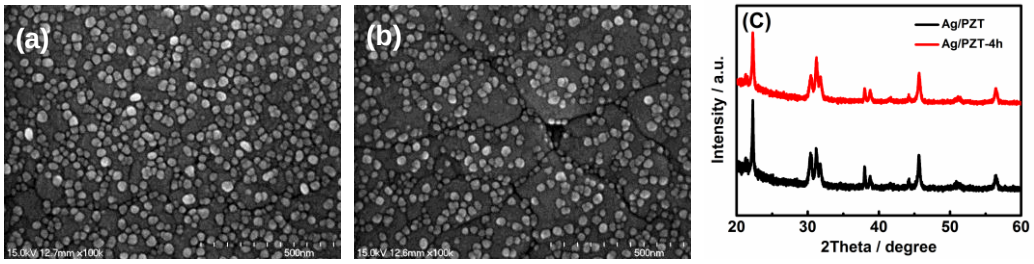

Fig. S6 The surface SEM of (a) the original Ag/PZT and (b) the one after 4 hours continuous PEC measurement. (c) The XRD of the corresponding samples.

S7: Tuning of V_{oc} by polarization switching.

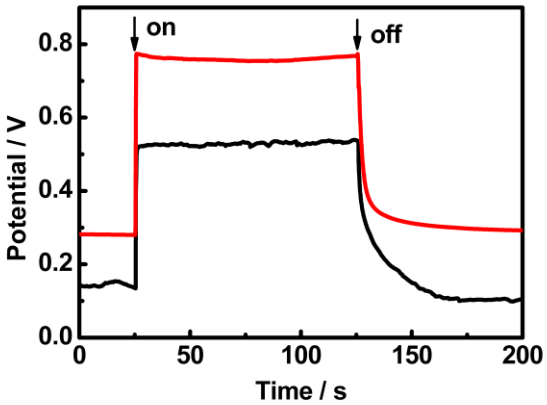

Fig. S7 The open-circuit voltage vs time curves for the Ag/PZT sample with the ferroelectric PZT film under polarization-right (red curve) and –left (black curve).

This journal is © The Royal Society of Chemistry 2013

S8: The measurement of H_2 evolution in the photocathode

To measure and/or observe the production of H_2 gas, we home-made a gas generation and collection system using quartz tubes, which is similar to that described by Zhang et al. (Nano Lett., nl3029202), as presented in Figure S8a. In the photo-reactor, the photocathode (ITO/PZT/Ag) and the counter electrode (Pt wire) were separated in different tubular chambers, which avoid the mixing of hydrogen generated on the photocathode and oxygen on the Pt counter electrode. SCE electrode was used as a reference electrode. The hydrogen and oxygen gases can be separately collected, taken out by a small syringe, and measured by a gas chromatography (GC) (Tianmei, GC 7890T, made in China). The Quartz tube was filled with 0.1M Na_2SO_4 electrolyte solution. A small amount of bubbles can be seen nucleating on the photoelectrode and Pt surface within several minutes and more bubbles are formed on the surface as time increases. During the relatively long time (120 min) measurement, bubbles are clearly observed to evolve from the photocathode and Pt counter electrode. In the revised manuscript, the digital photographs showing hydrogen and oxygen bubbles have been added to Figure S8c and S8e respectively in Supporting Information. The production of H_2 on the photocathode was confirmed by the GC measurements and it increases as time increases. However, on account of experimental difficulty concerning accumulation of the small amount of H_2 gas which diffuses to the top of the cell and partially adsorbs by the electrolyte, we are not able to determine the Faradic efficiency at this moment. We will try to develop the appropriate method to do so in the future.

This journal is © The Royal Society of Chemistry 2013

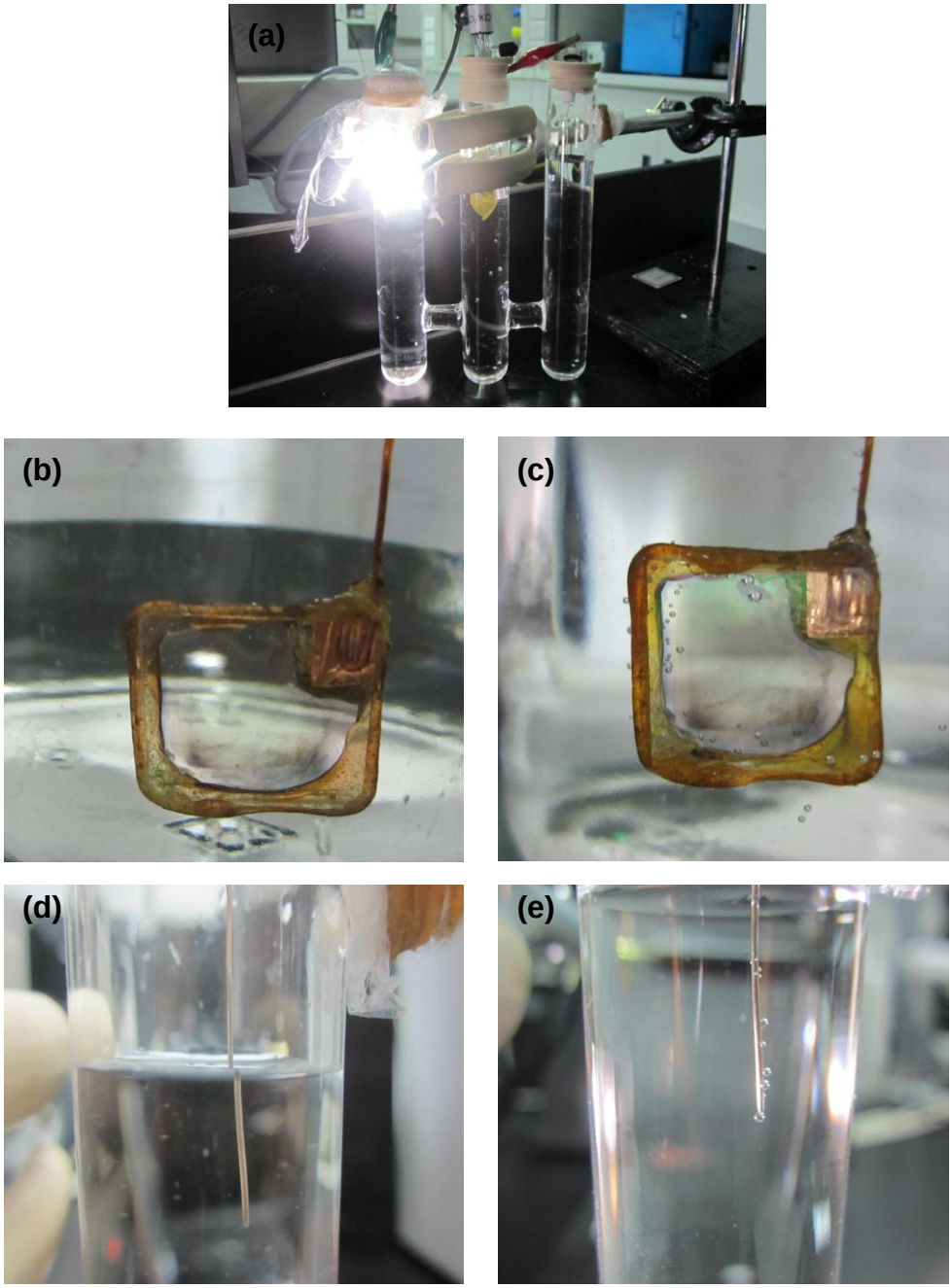

Fig. S8 (a) The digital photo of the homemade gas generation and collection system. The photocathode (b) before illumination and (c) just after illumination for 1h. The Pt wire (d) before illumination and (e) just after illumination on the photocathode. Bubbles can be seen on both the photocathode and Pt wire after illumination.

This journal is © The Royal Society of Chemistry 2013

References:

1 J. B. Gao, C. L. Perkins, J. M. Luther, M. C. Hanna, H. Y. Chen, O. E. Semonin, A. J. Nozik, R. J. Ellingson and M. C. Beard, *Nano. Lett.*, 2011, **11**, 3263.

2 M. Qin, K. Yao, Y. C. Liang and B. K. Gan, *Appl. Phys. Lett.*, 2007, **91**, 092904.

3 Y. Park, V. Choong, Y. Gao, B. R. Hsieh and C. W. Tang, *Appl. Phys. Lett.*, 1996, **68**, 2699.

4 F. Nuesch, L. J. Rothberg, E. W. Forsythe, Q. T. Le and Y. L. Gao, *Appl. Phys. Lett.*, 1999, **74**, 880.

5 N. Wang, X. X. Liu and X. Y. Liu, *Adv. Mater.*, 2010, **22**, 2211.

6 M. G. Helander, Z. B. Wang, J. Qiu, M. T. Greiner, D. P. Puzzo, Z. W. Liu and Z. H. Lu, *Science*, 2011, **332**, 944.